SLAC-PUB-1242
(T/E)
May 1973

A STUDY OF HADRONIC FINAL STATES FROM INELASTIC MUON SCATTERING IN A HYBRID BUBBLE CHAMBER EXPERIMENT*

Michel Della Negra†
Stanford Linear Accelerator Center
Stanford University, Stanford, California 94305

ABSTRACT

A study of general features of charged hadron production by inelastically scattered 16 GeV muons detected in the SLAC rapid cycling 40" hydrogen bubble chamber is presented.

I. INTRODUCTION

Scaling of the structure function νW_2 in inelastic electron scattering has been experimentally verified over an impressive range of momentum transfer, Q^2, in the single arm spectrometer experiments at SLAC.[1] What is even more intriguing is that scaling holds already (precocious scaling) at $Q^2 \simeq 1$ GeV^2 and $W \simeq 2$ GeV, if one uses the scaling variable $\omega' = 1 + W^2/Q^2$, where W is the c.m. mass at the hadronic vertex. In this Q^2 and W range the cross sections are not yet ridiculously small, and it is possible to observe the spectra of hadrons associated with the scattered lepton using the 4π acceptance (for hadrons) of a bubble chamber. One could hope to learn more about this very simple experimental result, by looking directly at the hadronic spectrum undetected in the single arm experiment.

In Ref. 2 a preliminary analysis based on ~50% of the full data was given. The data reported today is complete; however the analysis is still preliminary. The experiment and analysis was performed by the authors of Ref. 2.

We used the SLAC 40" hydrogen bubble chamber running at 10 expansions per second with the camera flash triggered by the scattered lepton. In a bubble chamber we cannot use an electron beam because it would fill the pictures with unwanted e^+e^- pairs from converted γ rays. We thus constructed a 16 GeV μ^- beam.

II. EXPERIMENTAL SETUP

A schematic representation of the experiment is shown in Fig. 1. The beam uses μ's produced at 0° and transported through 3 foci with a 3.7 meter Be filter at the first focus. The trigger is defined by 4 sets of scintillation counters, S1, S2, S3, S4 surrounding the beam. S1 and S2 are two veto counters in front of the bubble chamber to reject beam halo, while S3 and S4 behind detect muons with a nominal scattering angle $\gtrsim 1.4^\circ$. Seven

---

*Work supported by the U. S. Atomic Energy Commission.
†On leave from College de France, Paris.

(Presented at the International Conference on New Results from Experiments on High Energy Particle Collisions, Vanderbilt University, Nashville, Tenn., March 26-28, 1973.)

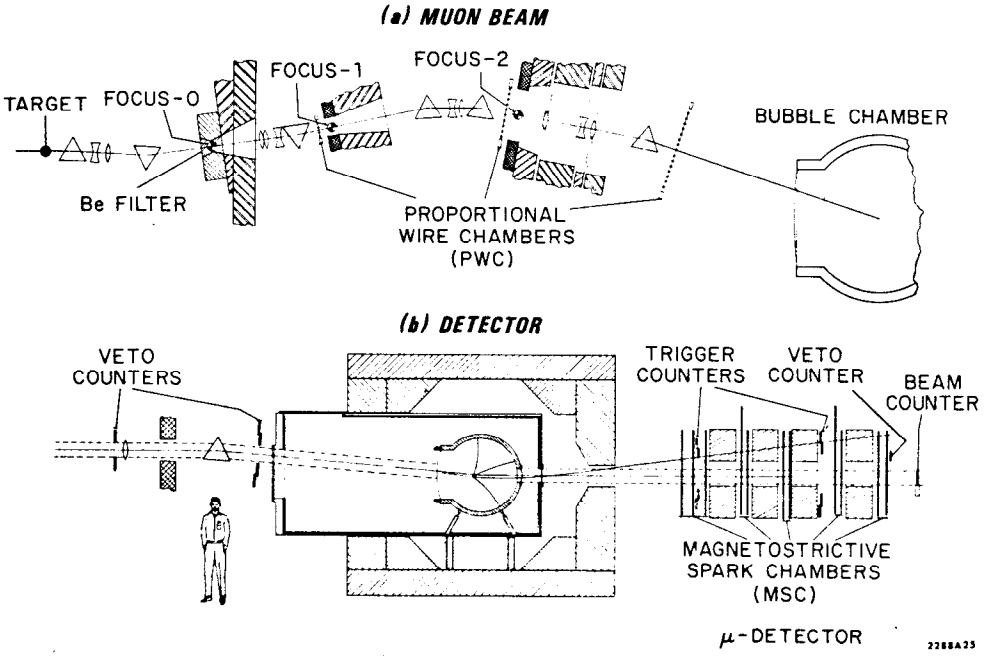

Fig. 1. Schematic representation of the experiment.

collision lengths of iron between S3 and S4 provide the fast identification of a muon. The trigger is then $\overline{S1}\cdot\overline{S2}\cdot S3\cdot S4$. In addition to the triggered bubble chamber picture, we record on a magnetic tape the trajectory of the scattered muon, using 11 1m × 1m magnetostrictive spark chambers. This information is used off-line for the final signature of the good μ events and for a more precise reconstruction of the scattered μ track. The final π contamination of the selected sample was measured to be < 1% by runs taken with a reduced length of Be filter in the beam.

Table I summarizes the properties of the μ^- beam and the event and picture rates.

Table I Beam Parameters and Event Rates

μ^- Beam		Event Rates
Momentum	16.0	30 millions expansions at
Momentum spread	±0.6 GeV/c (±3.7%)	10 expansions per second
Intensity	100 μ's/pulse	100 μ's per pulse
Vertical size	11 cm FWHM	
Horizontal size	1.2 cm FWHM	94,000 triggered pictures
Vertical divergence	4 mrad FWHM	4922 useful good μ events
Horizontal divergence	3.5 mrad FWHM	1181 elastics (24%)
Penetrating halo	2%	3741 inelastics (76%)
Measured contamination	$\pi/\mu < 5 \times 10^{-5}$	

III. RESULTS

The process

$$\mu^- p \rightarrow \mu^- + \text{hadrons} \qquad (1)$$

can be understood as a two-step process: (i) The exchange of a virtual photon γ_v, of laboratory energy ν, and mass squared $q^2 = -Q^2 < 0$; (ii) followed by the reaction

$$\gamma_v p \rightarrow \text{hadrons} \qquad (2)$$

with center-of-mass energy squared

$$s = W^2 = M_p^2 + 2 M_p \nu - Q^2$$

where M_p is the mass of the proton. The kinematics of the process and in particular the relation between the structure functions W_2 and W_1, and the total cross section for reaction (2) is described in the literature.[1,2]

The kinematic range of our data is

$$M_p < W < 5 \text{ GeV}$$

$$0.05 < Q^2 < 3 \text{ GeV}^2 .$$

So we can study well the transition region between photoproduction ($Q^2 = 0$) and the scaling region ($W > 1.8$ GeV, $Q^2 > 1$ GeV^2). The photoproduction data used for comparison are extracted from Ref. 3.

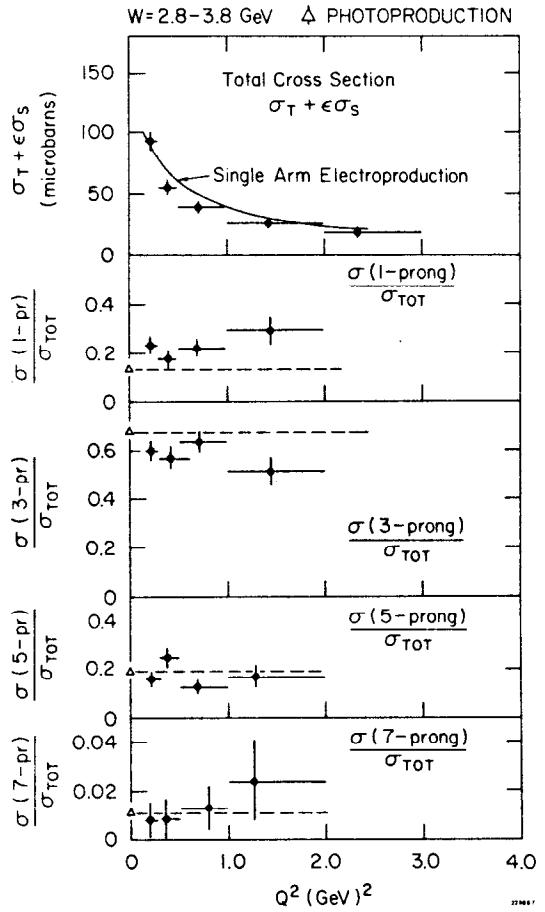

Fig. 2. Total cross section value $\sigma_T + \epsilon\sigma_S$. The solid line is the single arm electroproduction cross section averaged over the same W range. Below, each point is broken into fractional contributions from different topologies.

A. Total Cross Section and Topological Cross Sections

We have measured the total cross section σ_{tot} as a function of W and Q^2 and have compared our results with the precise measurements of the single arm experiment[1] in Fig. 2 (top) for the particular range $2.8 < W < 3.8$ GeV. ($\langle W \rangle = 3.25$ GeV.) Here as in other ranges our measured total cross section is in satisfactory agreement (to 10%) with the measurements of Ref. 1. Figure 2 also displays the different topological contributions to the cross sections, σ_n/σ_{tot} as a function of Q^2. We shall define n as the number of charged

hadrons (prongs) in analogy to photoproduction studies. At this energy the main contributions come from the 3-prongs. One sees from Fig. 2 that the relative contributions of the 1-prong and the 3-prong vary with Q^2. In particular, the 1-prong contribution is consistently greater than in photoproduction and seems to increase with Q^2, while the 3-prong fraction is (necessarily) smaller than in photoproduction. A similar variation is observed in the whole range $1.8 < W < 5$ GeV.

B. Charged Hadronic Multiplicities

Another way to study the above effect is to look at the mean charged multiplicity

$$\langle N \rangle = \frac{\Sigma n \sigma_n}{\Sigma \sigma_n} = \frac{\Sigma n \sigma_n}{\sigma_{tot}}$$

as a function of W and Q^2.

We first study <N> as a function of Q^2 for fixed W ranges. The results are shown in Fig. 3 for three intervals. <N> decreases slightly as Q^2 increases for each W range. Since in photoproduction <N> increases with s at fixed Q^2 as well as in this experiment, it is tempting to look for a possible scaling of <N>, for example, as a function of $\omega' = 1 + s/Q^2$.

To do this we plot <N> versus $\ell n\, Q^2$ for two ω' intervals: $3 < \omega' < 5$ and $5 < \omega' < 10$. At fixed ω', s grows with Q^2 and a ℓn s behavior of <N> would force the data points to be on a straight line with positive slope. The result is shown in Fig. 4, where below each point we give the mean value of W for the interval used. The dashed line in each case indicates the mean multiplicity found in photoproduction for these values of W.

If <N> were independent of Q^2, the points would fall on the dashed line. If <N> scales with ω', it should be independent of Q^2 on such a plot. The data show a possible levelling off of <N>, starting at $Q^2 = 1$ GeV^2, which may encourage the scaling enthusiast.

To further illustrate this point we show, in Fig. 5, <N> as a function of

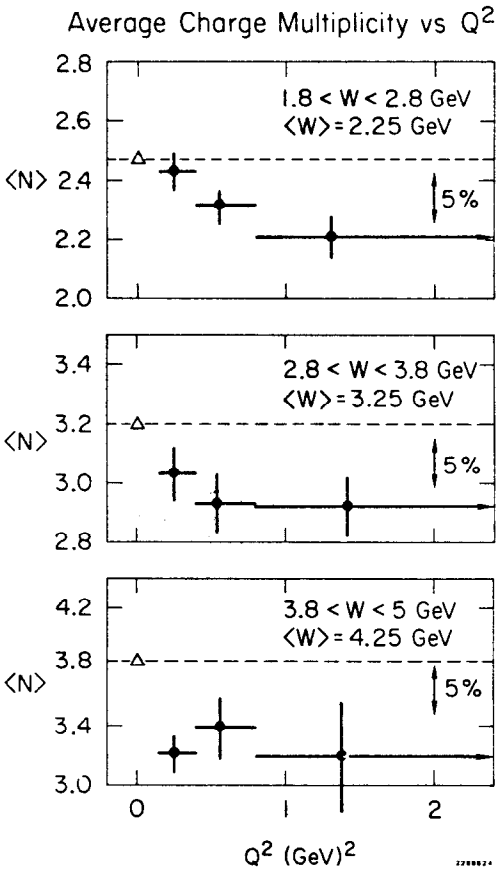

Fig. 3. The charged hadronic multiplicity as a function of Q^2 at fixed W.

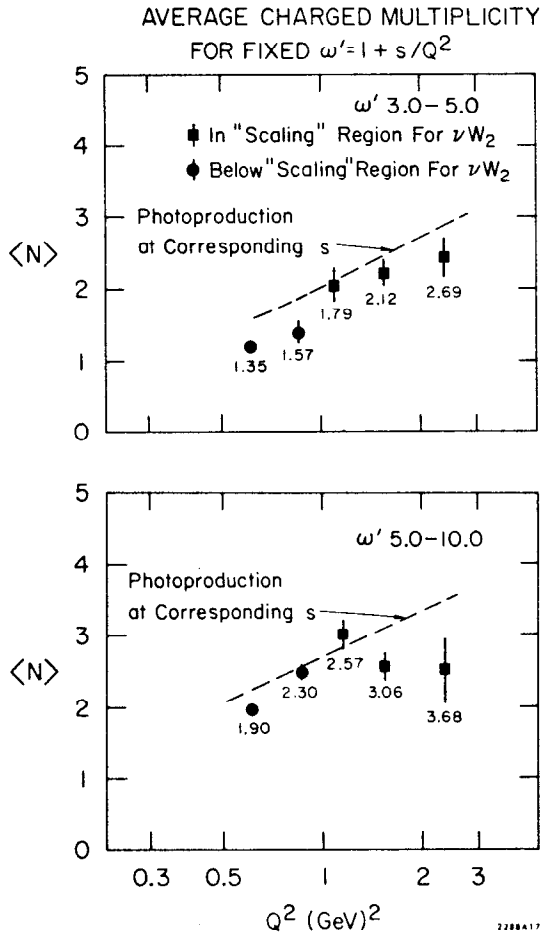

Fig. 4. The charged hadronic multiplicity as a function of Q^2 for two ω' intervals. The mean value of W is shown below each data point. The dashed line is the photoproduction multiplicity ($Q^2=0$) at the corresponding W.

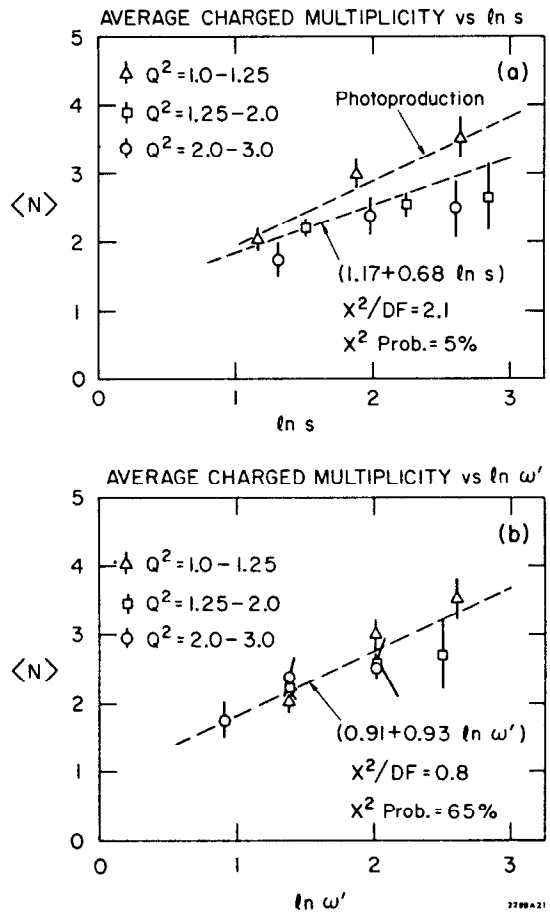

Fig. 5. a) The charged hadronic multiplicity as a function of ℓn s for the Q^2 intervals shown. b) The charged hadronic multiplicity as a function of ℓn ω'.

ℓn s and ℓn ω'. The dashed lines correspond to best fits to a straight line. The results are, for 7 degrees of freedom:

$$\langle N\rangle = (0.68\pm0.15)\ \ell n\ s + (1.17\pm0.27);\quad \chi^2 = 14.5;\ \text{Prob}\ (\chi^2) = 5\%$$

$$\langle N\rangle = (0.93\pm0.17)\ \ell n\ \omega' + (0.91\pm0.28);\quad \chi^2 = 5.6;\ \text{Prob}\ (\chi^2) = 65\%\ .$$

The photoproduction line does not fit the data, while the ℓn ω' behavior is slightly favored.

C. Charge Ratio n_+/n_-

It has been observed in a previous experiment at SLAC by J. Dakin et al.,[4] that the inclusive charge ratio n_+/n_- (number of positively charged hadrons divided by number of negatively charged hadrons) increases with Q^2

in the region $0.3 < x < 1.0$, defined in the hadron c.m.s., where x is the Feynman inclusive variable

$$x = p^*_{\parallel}/p^*_{max} \quad .$$

Figure 6 shows the charge ratio as a function of Q^2 for $W > 2.5$ GeV and for different x regions. Here we see that the charge ratio increases with Q^2 in the forward region $0.3 < x < 1.0$, in agreement with Dakin et al.,[4] but is relatively constant in other x regions. We note here that the charge ratio is related to multiplicity. Charge conservation requires $n_+ - n_- = 1$, i.e., $n_+/n_- = 1 + 1/n_-$. Hence the observed decrease in total multiplicity, as described in the preceding section, requires n_+/n_- to increase with Q^2 when averaged over the whole range of x. Thus both effects are related to variations in the photon fragmentation region.

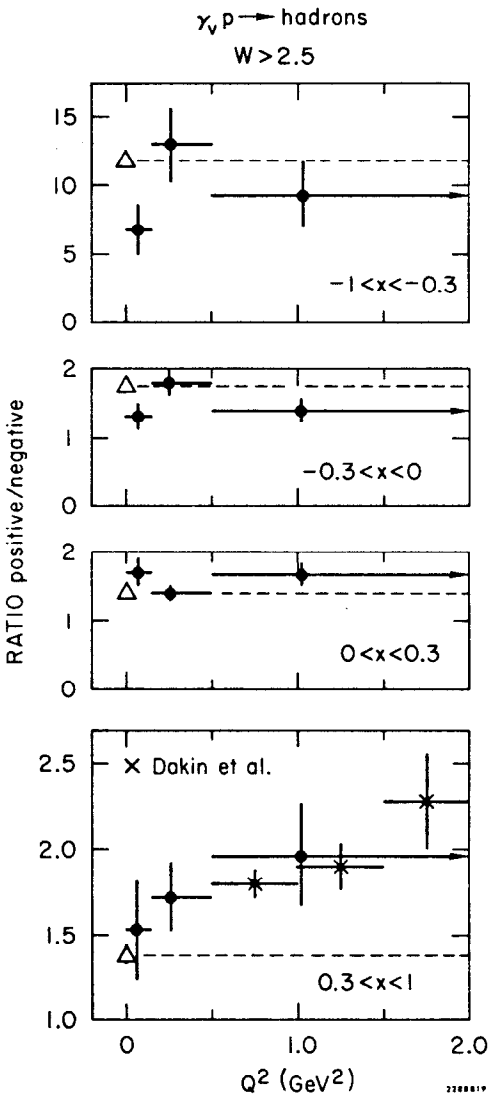

Fig. 6. The charge ratio as a function of Q^2 for various x ranges.

D. Inclusive $\pi^{\pm}$ Distribution

The differential cross section for the inclusive reaction

$$\gamma_v p \rightarrow \pi \ + \text{(anything)}$$

can be expressed as

$$d^2\sigma = \pi \frac{p^*_{max}}{E^*} \, dx \, dp_\perp^2 \, f\left(x, p_\perp^2, s, Q^2\right)$$

The structure function $f(x, p_\perp^2, s, Q^2)$ is in general a function of s and Q^2. At $Q^2 = 0$ we know that the s dependence is already weak at moderate energy,[3] i.e., approximate Feynman scaling. We now investigate the Q^2 dependence.

1. x-dependence

First we integrate over $p_\perp^2$ and show the integrated structure function $F(x, s, Q^2)$ normalized to the total cross section for two W and Q^2 bins in Fig. 7 for the π^- and in Fig. 8 for the π^+. The dashed line is the corresponding structure function for photoproduction ($Q^2 = 0$).

The structure functions for virtual and real photoproduction agree very well for $x < 0.3$ and hence have there only weak s and Q^2 dependences. For $0.3 < x < 1$, which may be considered the photon fragmentation region, the

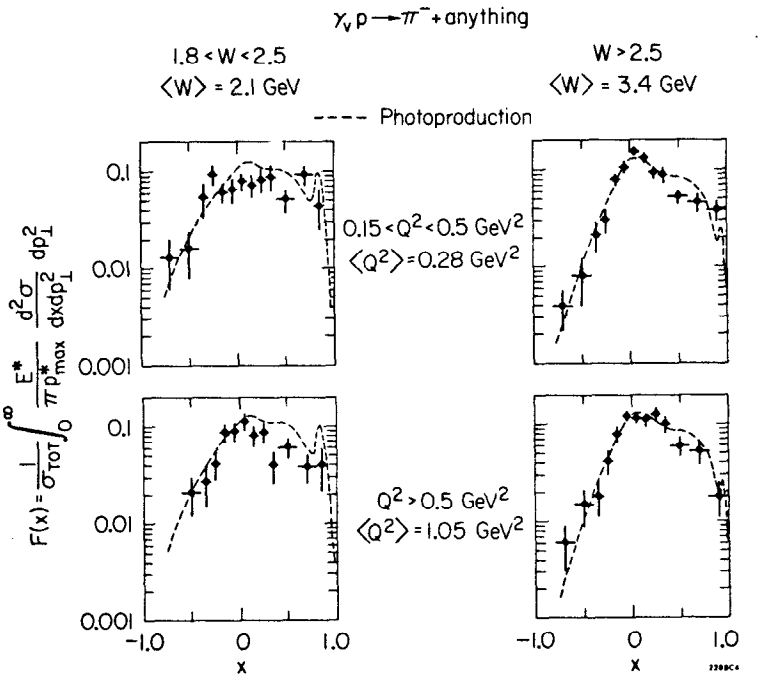

Fig. 7. Reaction $\gamma_V p \rightarrow \pi^- +$ anything: normalized structure function F(x) vs x.

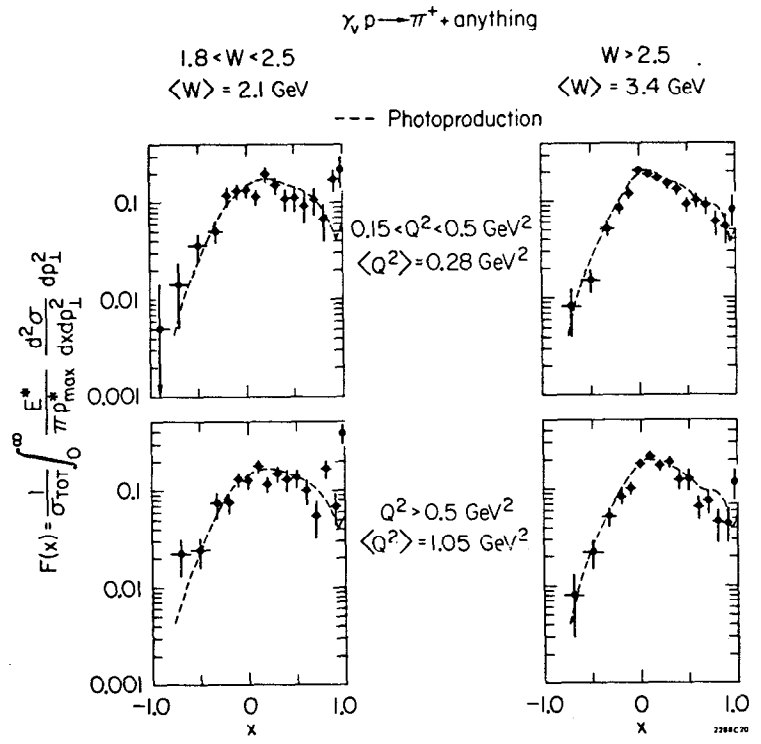

Fig. 8. Reaction $\gamma_V p \rightarrow \pi^+ +$ anything: normalized structure function F(x) vs x.

situation appears more complex. The peaks in the dashed curve decrease in prominence with increased s (these are due to two-body channels like πN and $\pi\Delta$ production), while for $Q^2 > 0$ they appear to decrease more slowly, especially in the π^+ case. Aside from this effect, there is a tendency for the $Q^2 \neq 0$ points to be on the average lower than in photoproduction in this x region.

Part of this Q^2 dependence of the inclusive spectrum can be attributed to the exclusive channels like

$$\gamma_v p \to \rho^o p$$

$$\gamma_v p \to \pi^+ n, \quad \pi^+ \Delta^o, \quad \pi^- \Delta^{++}$$

which will be discussed later.

2. $p_\perp$ dependence

Next we integrate over x and discuss the $p_\perp^2$ distributions. These are roughly $\propto \exp(-B p_\perp^2)$ and we describe them by the slope parameter

$$B = \langle p_\perp^2 \rangle^{-1}$$

Figures 9 and 10 show B as a function of Q^2 for two s intervals for the π^- and π^+.

At low W, the comparison with photoproduction is difficult (the photoproduction value of B is shown by a triangle) because B depends strongly on W in the region $1.8 < W < 2.5$ GeV. We thus discuss only the region $W > 2.5$ GeV for which the photoproduction value does not change much with W. From a comparison with photoproduction we learn that B does not vary with Q^2 in the central region $-0.5 < x < 0.5$ and B

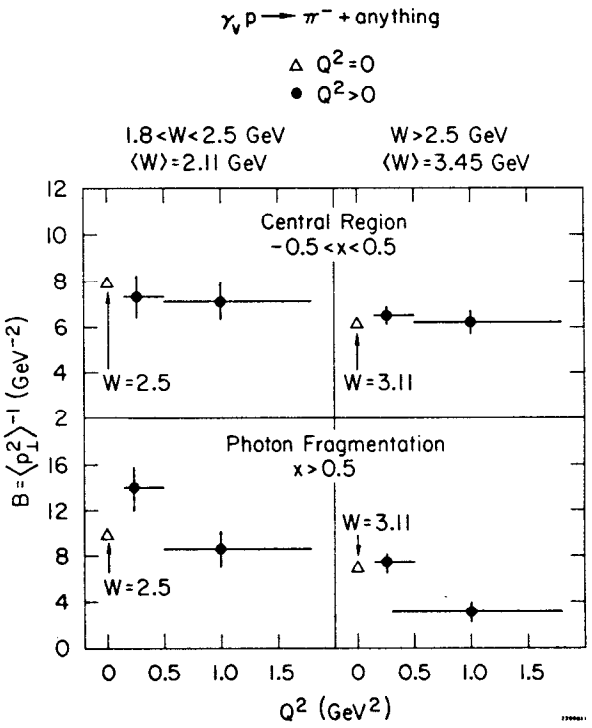

Fig. 9. Reaction $\gamma_v \to \pi^-$ + anything: the slope parameter $B = \langle p_\perp^2 \rangle^{-1}$ vs Q^2.

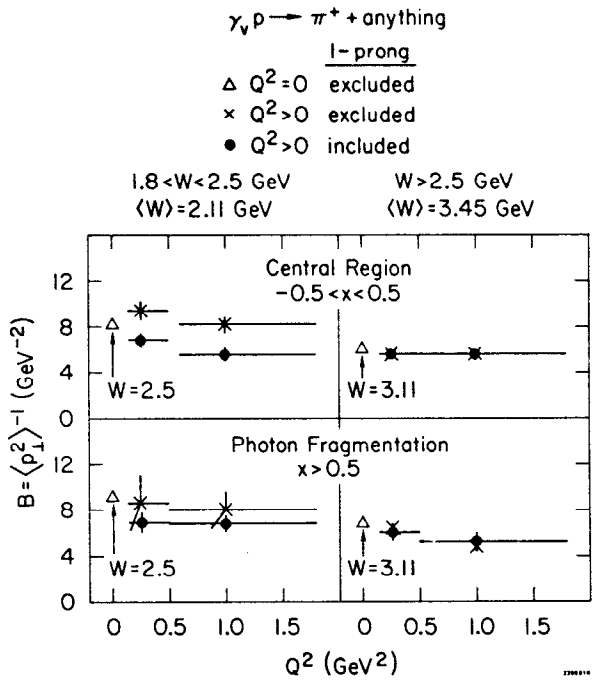

Fig. 10. Reaction $\gamma_v \to \pi^+$ + anything: the slope parameter $B = \langle p_\perp^2 \rangle^{-1}$ vs Q^2.

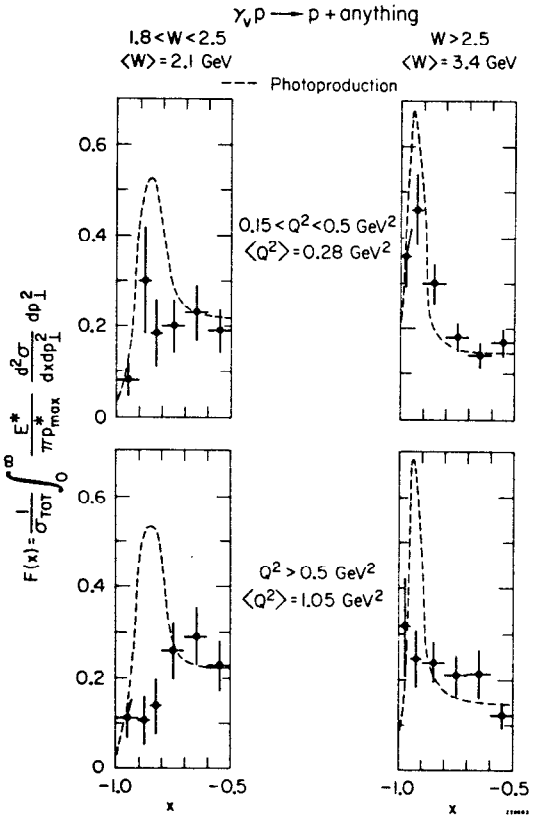

Fig. 11. Reaction $\gamma_v p \rightarrow p +$ anything: normalized structure function F(x) vs x.

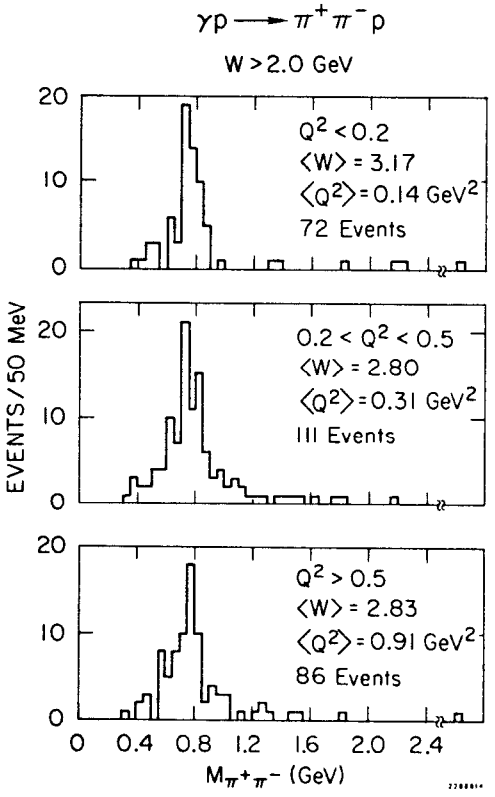

Fig. 12. The dipion mass spectrum for the reaction $\gamma_v p \rightarrow p\pi^+\pi^-$ for W > 2 GeV.

seems to decrease with Q^2 in the photon fragmentation region now taken to be $0.5 < x < 1.0$. This may indicate "photon shrinkage."

E. Diffractive Backward Protons

Figure 11 shows F(x) for slow laboratory protons $-1 \leq x \leq -0.5$, for two W bins and two Q^2 bins. The dashed line is the corresponding structure function as measured in photoproduction. In photoproduction the strong peak near $x \sim -1$ comes mainly from the diffractive process $\gamma p \rightarrow p\rho^0$.

The diffractive peak disappears as Q^2 increases. This effect can be studied directly by looking at the exclusive channel

$$\gamma p \rightarrow p\pi^+\pi^- \quad .$$

Figure 12 shows the effective mass $M(\pi^+\pi^-)$ spectrum as a function of Q^2. From a maximum likelihood fit to this channel we can extract the cross section σ_ρ for the diffractive process $\gamma p \rightarrow p\rho^0$. On Fig. 13, we show the ratio σ_ρ/σ_{tot} as a function of Q^2. The triangle is the photoproduction point; σ_ρ/σ_{tot} decreases as Q^2 increases.

F. Correlations in $p_\perp$ plane

Our last topic will be the search for exotic events showing a jet structure in the plane perpendicular to the virtual photon. In this plane the ith charged particle (i = 1, N) is described by its azimuth angle ϕ^i with respect to the μ scattering plane and transverse momentum $\vec{p}_\perp^{\,i}$. R. N. Glasser has introduced a variable which is sensitive to jet-like structures.[5] For each event one computes:

$$T = \frac{\left(\sum_{i=1}^{N} p_\perp^i \cos 2\phi^i\right)^2 + \left(\sum_{i=1}^{N} p_\perp^i \sin 2\phi^i\right)^2}{\left(\sum_{i=1}^{N} p_\perp^i\right)^2}$$

(sum on N charged particles only)

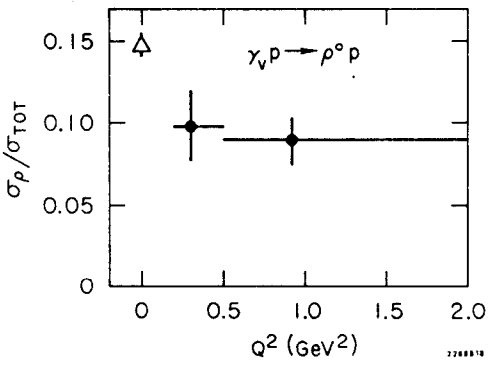

Fig. 13. Ratio of the cross section σ_ρ for the reaction $\gamma_v p \rightarrow p\rho^o$ to the total cross section σ_{tot} vs Q^2 (W > 2 GeV).

T varies between 0 and 1; a pure jet would have

$$\phi^i = \phi^j \pm \pi \qquad j \neq i = 1, 2, \ldots N \text{ implying } T = 1$$

If all ϕ^i's are uncorrelated then, on the average, $\langle T \rangle \simeq 1/N$ where N is the number of charged particles. Jet events would show a peak at $T \simeq 1$ on a T distribution having a maximum near T = 0.

Figure 14 shows T distributions for different multiplicities. The left hand side is for real photoproduction events at W = 3.1 GeV, while the right hand side is for virtual photoproduction for all Q^2 and W > 1.8 GeV. The solid line is the distribution expected for no real correlations, but with momenta constrained by transverse momentum conservation. The peak at T = +1 observed at low multiplicity (3 charged, no neutral) is due to momentum conservation. At higher multiplicity, no strong peak is observed at T = +1. However, for the topology 3 charged, $\geq$ 1 neutral, a small effect is possible. For these events, we divide the Q^2, ν plane into two regions of the scaling variable ω:

(a) high ω events defined by the cut $\nu > 3 + 5\ Q^2$,

(b) small ω events defined by the cut $\nu < 3 + 5\ Q^2$.

Figure 15 shows the T distribution. The peak at T = 1 is found concentrated in the low ω events, which could be an indication that some jet production is present.

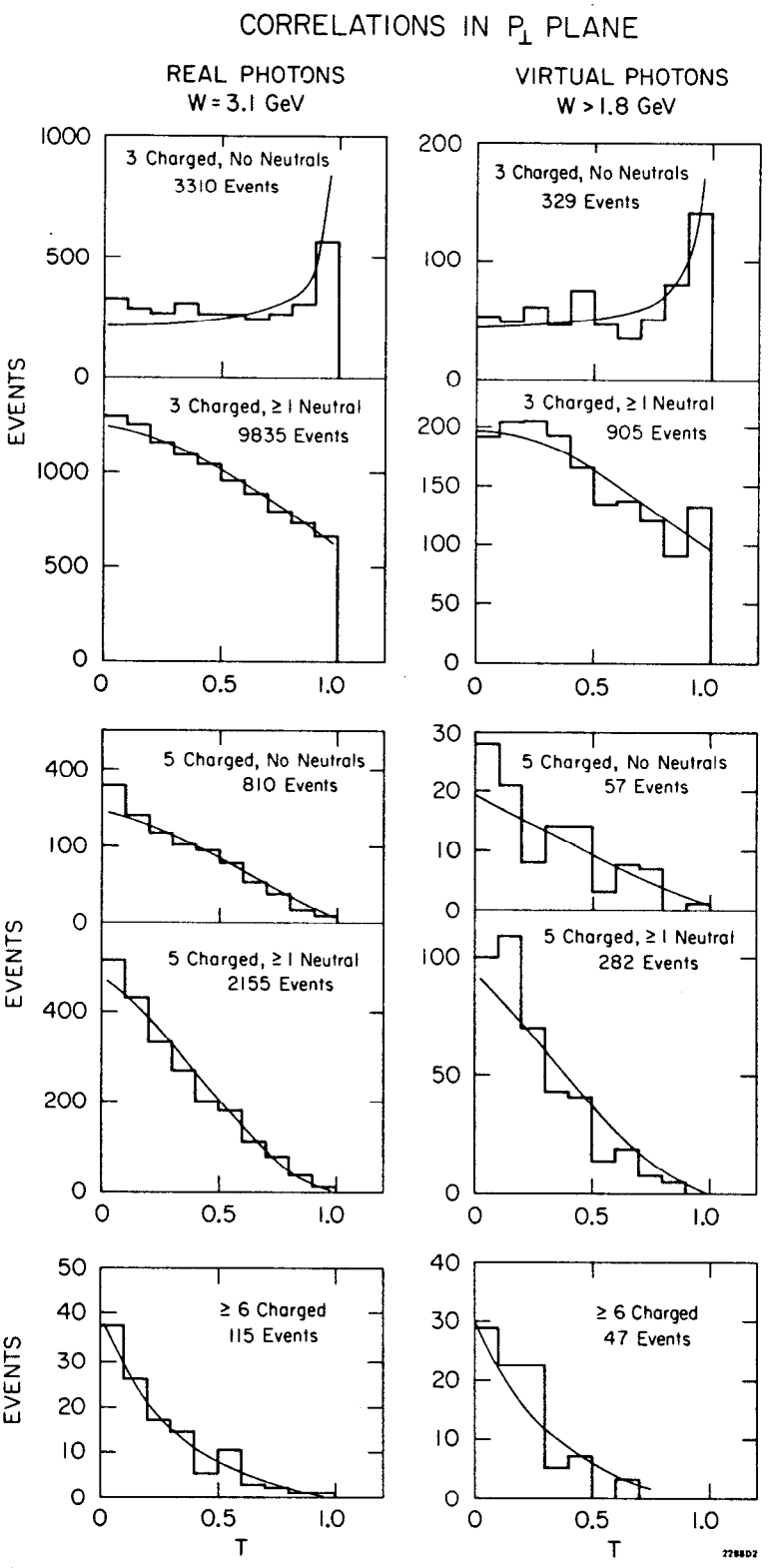

Fig. 14. Search for "jet-like" structure in various prong numbers. T is defined in the text: A jet should cause a peak at T = 1.

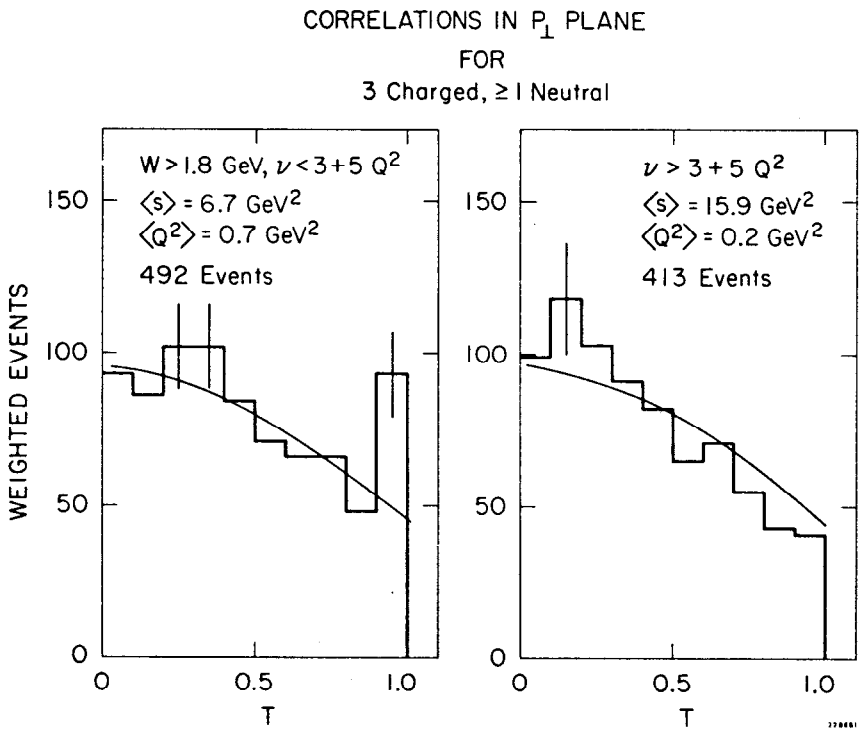

Fig. 15. T distribution for the events with 3 charged, ≥ 1 neutral.

IV. CONCLUSIONS

1. The charged multiplicity suggests that scaling behavior in ω' may be beginning at $Q^2 \gtrsim 1\ GeV^2$.

2. The positive to negative charge ratio increases with Q^2, but only in the forward direction ($0.3 < x < 1$).

3. The normalized $\pi^\pm$ inclusive distributions show little s and Q^2 dependence when divided by the total cross section, except in the forward direction ($0.3 < x < 1$).

4. The diffractive backward proton peak disappears as Q^2 increases. The particular diffractive channel $\gamma_V p \rightarrow p\rho^0$ has a decreasing contribution to the total cross section as Q^2 increases.

5. No prominent jet-like structure events in the transverse momentum plane are found. However, a three-standard deviation effect in one topology is suggested for events with small ω (i.e., those closest to the deep inelastic scattering region.

ACKNOWLEDGEMENTS

We thank Bob Watt and the bubble chamber operations crew for the operation of the 40-in. HBC at 10 pps without which this experiment would not have been possible. The suggestions and help of Dr. Eliezer Kogan,

Dr. William Johnson and Dr. Jerry Friedman of SLAC are gratefully acknowledged. Also, we thank Kenneth Eynman and Dennis Feick for their help in the data reduction and programming. The careful scanning and accurate measuring efforts of the scanners of CDA and the help of Marie La Belle was most essential for the success of this experiment.

REFERENCES

1. G. Miller et al., Phys. Rev. D 5, 528 (1972) and earlier references contained therein.
2. J. Ballam, E. D. Bloom, J. T. Carroll, G. B. Chadwick, R.L.A. Cottrell, M. Della Negra, H. DeStaebler, L. K. Gershwin, L. P. Keller, M. D. Mestayer, K. C. Moffeit, C. Y. Prescott, S. Stein, Report No. SLAC-PUB-1163, Stanford Linear Accelerator Center (1972).
3. (a) Preliminary results from Group A, LBL; private communication from H. Oberlock (August 1972).
   (b) SLAC-LBL-Tufts collaboration: J. Ballam et al., Phys. Rev. D 5, 545 (1972); K. Moffeit et al., Phys. Rev. D 5, 1603 (1972). Some photoproduction results shown here have not yet been published and were obtained using the SLAC-LBL-Tufts data summary tapes.
4. J. T. Dakin et al., Phys. Rev. Letters 29, 746 (1972).
5. R. N. Glasser, NAL internal note (unpublished).